Science of the Total Environment 545–546 (2016) 654–661

Contents lists available at ScienceDirect

Science of the Total Environment

journal homepage: www.elsevier.com/locate/scitotenv

Mapping the spatial distribution and activity of ^{226}Ra at legacy sites through Machine Learning interpretation of gamma-ray spectrometry data

Adam Varley [a,*], Andrew Tyler [a], Leslie Smith [b], Paul Dale [c], Mike Davies [d]

[a] Department of Biological and Environmental Sciences, University of Stirling, Stirling FK9 4LA, United Kingdom
[b] Department of Computing Science and Mathematics, University of Stirling, Stirling FK9 4LA, United Kingdom
[c] Scottish Environmental Protection Agency, Radioactive Substances, Strathallan House, Castle Business Park, Stirling FK9 4TZ, United Kingdom
[d] Nuvia Limited, The Library, Eight Street, Harwell Oxford, Didcot, Oxfordshire OX11 0RL, United Kingdom

HIGHLIGHTS

- Land contaminated with radium is hazardous to human health.
- Contamination characterised with gamma-ray spectrometry.
- Machine Learning to derive activity and depth estimated from spectral shape.
- Lanthanum bromide and Neural Network provided optimum performance.
- The developed approach demonstrates a powerful assaying tool.

GRAPHICAL ABSTRACT

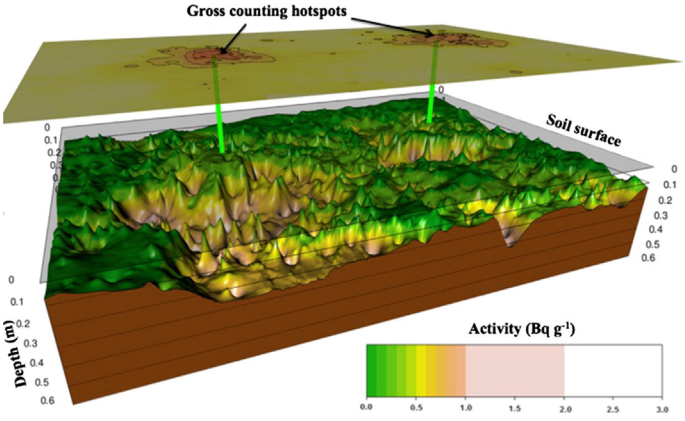

ARTICLE INFO

Article history:
Received 17 July 2015
Received in revised form 19 October 2015
Accepted 22 October 2015
Available online xxxx

Editor: D. Barcelo

Keywords:
Radium contaminated land
Gamma-ray spectrometry
Machine Learning
Contamination mapping

ABSTRACT

Radium (^{226}Ra) contamination derived from military, industrial, and pharmaceutical products can be found at a number of historical sites across the world posing a risk to human health. The analysis of spectral data derived using gamma-ray spectrometry can offer a powerful tool to rapidly estimate and map the activity, depth, and lateral distribution of ^{226}Ra contamination covering an extensive area. Subsequently, reliable risk assessments can be developed for individual sites in a fraction of the timeframe compared to traditional labour-intensive sampling techniques: for example soil coring. However, local heterogeneity of the natural background, statistical counting uncertainty, and non-linear source response are confounding problems associated with gamma-ray spectral analysis. This is particularly challenging, when attempting to deal with enhanced concentrations of a naturally occurring radionuclide such as ^{226}Ra. As a result, conventional surveys tend to attribute the highest activities to the largest total signal received by a detector (Gross counts): an assumption that tends to neglect higher activities at depth. To overcome these limitations, a methodology was developed making use of Monte Carlo simulations, Principal Component Analysis and Machine Learning based algorithms to derive depth and activity estimates for ^{226}Ra contamination. The approach was applied on spectra taken using two gamma-ray detectors (Lanthanum

* Corresponding author.
E-mail address: a.l.varley@stir.ac.uk (A. Varley).

http://dx.doi.org/10.1016/j.scitotenv.2015.10.112

Bromide and Sodium Iodide), with the aim of identifying an optimised combination of detector and spectral processing routine. It was confirmed that, through a combination of Neural Networks and Lanthanum Bromide, the most accurate depth and activity estimates could be found. The advantage of the method was demonstrated by mapping depth and activity estimates at a case study site in Scotland. There the method identified significantly higher activity (<3 Bq g^{-1}) occurring at depth (>0.4 m), that conventional gross counting algorithms failed to identify. It was concluded that the method could easily be employed to identify areas of high activity potentially occurring at depth, prior to intrusive investigation using conventional sampling techniques.

1. Introduction

1.1. Regulation of radium contaminated land

Radium (^{226}Ra) was used extensively during the 20th century in military, industrial, and pharmaceutical products (Tyler et al., 2013). ^{226}Ra has a half-life of over 1600 years, and is the parent of an additional 8 radioactive elements that together produce a complex array of alpha, beta and gamma emissions (Pratt, 1993). Follow-up studies into the health implications of radium dial workers in the US typify the risks associated with long-term radium exposure (Stebbings, 2001). Within the UK, radium was used extensively as a composite in luminescent paint principally by the military during wartime periods. Prior to the Radioactive Substances Act 1960 (HMSO, 1996) vast inventories of waste were routinely burned and buried with little record presenting complex remediation challenges (Wilson et al., 2013).

A report published in 2012 by the UK government, conservatively estimated there to be 150–250 Radium Contaminated Legacy Sites (RCLS) linked to Ministry of Defence activities within the UK (DECC, 2012). Moreover, it was recognised that there could be as many as 1000 contaminated sites in the UK alone. Similar RCLS can be found across other parts of Europe and North America (IAEA, 1998).

a) UK legislation has now provided the Scottish Environmental Protection Agency (SEPA) with a framework to classify radioactively contaminated land and set guidelines to describe the amount of contamination that may give rise to significant harm to humans (The Radioactive Substances Act 1993 Amendment (Scotland) Regulations, 2011). Homogeneous contamination at RCLS in Scotland is controlled by the following criterion: An effective dose must not exceed 3 mSv per annum (Statutory Guidance to support the Radioactive Contaminated Land (Scotland) Regulations, 2008).

Homogeneous contamination can be defined as contamination that is dissociated or not in particulate form, which can vary significantly in activity over small spatial scales.

Surface flux measurements using dosimetry can be used to rapidly assess the effective dose at a site (IAEA, 1998). Yet, this measurement is somewhat limited in thoroughly assessing the activity and burial depth of homogeneous contamination, which tend to change significantly across a RCLS (Varley et al., 2015b). These factors are critical pieces of information for long-term remediation purposes, particularly at sites that are exposed to the public, where changes in site use or erosion events may occur increasing the risk of contact (Dale et al., 2013).Currently, not one Scottish legislation alone can be used to specifically outline an activity limit that must not be exceeded for suspected homogeneous contamination at a RCLS. Therefore, in this study we accept that ^{226}Ra should be treated under the exemption for Naturally Occurring Radioactive Materials declaring:

b) An activity must not exceed 10 Bq g^{-1}(The Radioactive Substances Act 1993 Amendment (Scotland) Regulations, 2011).

The discrete nature of the items that were initially disposed of can also lead to the formation of *hot particles*. At one RCLS at Dalgety Bay, Fife, Scotland, a diverse range of *hot particles* and historic artefacts (<70 MBq) has been found (Dale et al., 2013). If such items were to be picked up by a member of the public this may result in a significant committed dose (Tyler et al., 2013). A method for the real-time identification of ^{226}Ra containing *hot particles* at RCLS has been outlined in our previous work (Varley et al., 2015a).

In light of the uncertainties behind site formation and the lack of disposal records, once a RCLS has been identified the contamination should be systematically characterised to ascertain the risk it poses to long-term human health; thus going beyond limited surface dosimetry estimates (IAEA, 1998). In this paper we propose a method that can be rapidly and inexpensively deployed at a RCLS to provide accurate estimates of near-surface *homogenous* ^{226}Ra contamination depth, activity, and spatial distribution.

1.2. Environmental gamma-ray spectrometry

Handheld gamma-ray spectrometry (HGS) or mobile gamma-ray spectrometry, generally performed using inorganic scintillators, is often the cheapest and most robust technique of characterising RCLS (IAEA, 1998, 2003; Knoll, 2010; Dale et al., 2013; Read et al., 2013; Haddad et al., 2014). Using this method the spatial extent and activity of gamma-emitting radionuclides can be estimated using remote surface measurements without the need for time-consuming invasive methods (Tyler, 2008). Individual energy spectra produced during a survey are representative of the localised radiation field a detector has passed through (Beck et al., 1972).

For mapping purposes each spectrum can be post-processed using an algorithm to unfold spectral information (Kock et al., 2012). The first objective of this unfolding process is to identify whether there are characteristic signals from radium contamination (source), which typically differ in shape from background spectra. For example, notice characteristic peaks at 351, 609, 1120, 1764 and 2244 are generated by a radium source (Fig. 1A). However, source-background separation is often complicated by spatial fluctuations in background (^{40}K, and the ^{238}U and ^{232}Th series) and comparatively benign (^{137}C in the case of RCLS) radioelements, alongside variations in soil density and composition, which together introduce nuisance spectral changes (Runkle, 2006). Fagan et al. (2012) presents an informative review of the challenges associated with, and the techniques employed in, spectral classification.

Once a contaminated spectrum has been identified, the second aim is to identify spectral elements that are symptomatic of source burial depth and activity. Notice non-linear changes take place across the spectrum as the burial depth of a source varies: for example lower energy peaks are attenuated more relative to higher energy peaks with increasing burial depth (Fig. 1A).

The multiple photopeak method aims to capture this occurrence by calculating the area under two background-subtracted full energy peaks with the purpose of comparing the observed ratio to that of a calibrated one to estimate source burial depth and activity (Miller et al., 1994; Thummerer and Jacob, 1998, Haddad et al., 2014). Another method that utilises more spectral information is termed Full Spectral Analysis (FSA). FSA compares the spectral similarity of an obtained spectrum to a calibration library by a weighted least-squares fitting procedure

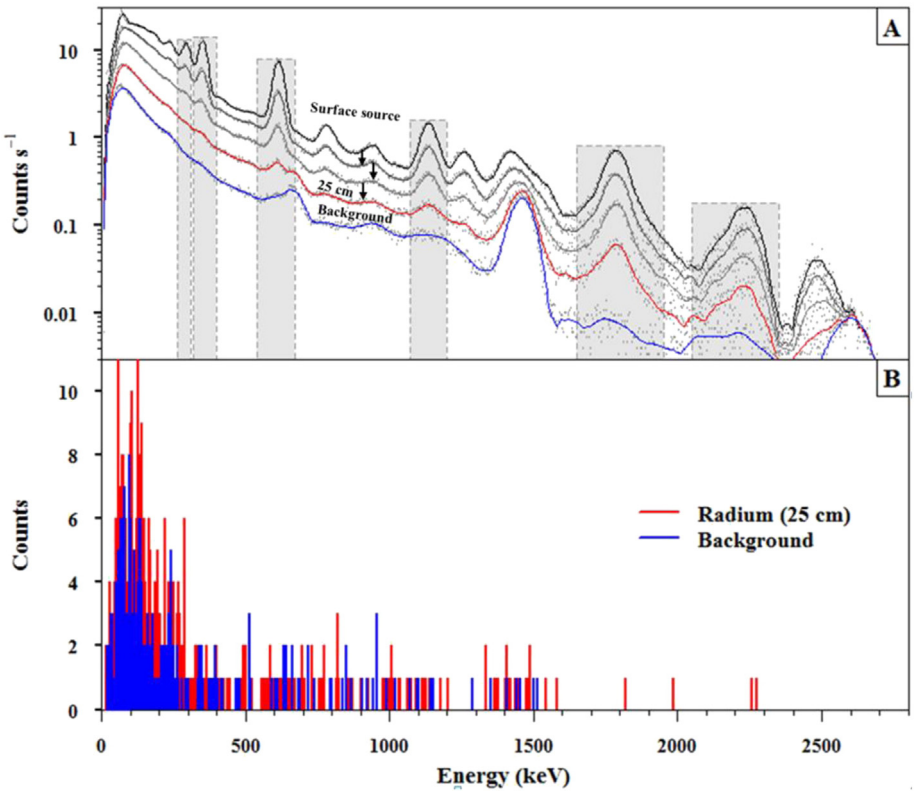

Fig. 1. A) Nonlinear spectral response as a function of homogeneous source burial depth and a typical background taken using 71 × 71 mm NaI:Tl detector. B) Spectra taken over 1 s demonstrating stochastic noise of background and 25 cm extended source.

using the majority of spectral channels (Hendriks et al., 2001; Caciolli et al., 2012; Guastaldi et al., 2013).

The practical application of to these methods is, however, somewhat limited by stochastic noise presented within individual spectra introduced as a consequence of the short count times required to map a RCLS in high resolution within a limited time period (IAEA, 1998; Alamaniotis et al., 2013a) (Fig. 1B). Subsequently, many HGS surveys fall back on unsophisticated spatial interpretation methods such as the total signal (Gross counting) where the highest activities are attributed to the highest count rates (Adsley et al., 2004). At the majority of RCLS, this assumption is known to break down and higher activities at greater depths fail to be acknowledged (Fig. 2). For example, a 0.1 Bq g^{-1} homogenous source at the surface will produce an identical signal to a 1 Bq g^{-1}

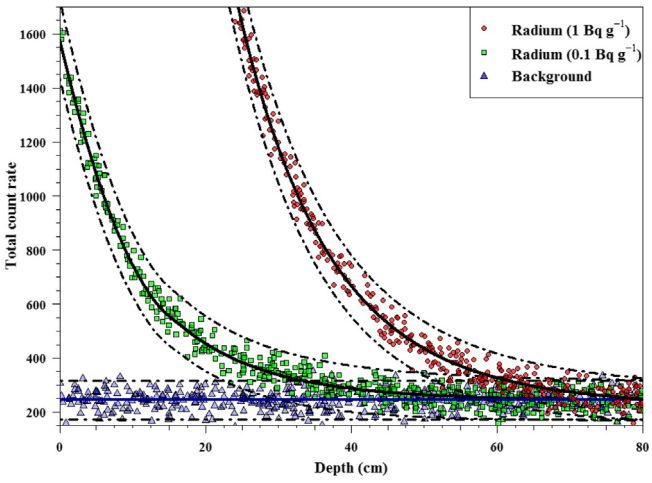

Fig. 2. Total signal from background, 0.1 and 1 Bq g^{-1} homogeneous sources as a function of burial depth.

homogenous source (radius 1 m) buried at approximately 40 cm. Furthermore, weaker source signal can easily be mistaken for background.

This paper investigates: i) whether improvements can be made into the identification and estimation of depth and activity of homogeneous ^{226}Ra contamination through *consideration of the distribution of counts across the spectrum*; and ii) whether the superior energy resolution of LaBr:Ce can demonstrate improvement compared to conventional NaI:Tl. This was achieved through a multivariate approach that develops the noise suppression and dimensionality reduction properties of the Principal Component Analysis (PCA) transform alongside the pattern recognition capabilities of Machine Learning (ML).

2. Material and methods

2.1. Field site and data collection

The case study site is found in Scotland, although its exact location cannot be disclosed and thus coordinates have been made anonymous and background maps are not included. The site has known to be associated with ^{226}Ra contamination for some time due to the historic disposal of military products. The exact physical form of contamination was not known and little information was available regarding the estimated inventory of the site. However, disposal of ^{226}Ra was known to have taken place over a number of years, particularly during and immediately after WWII, when a large number of military aircraft were dismantled. Large sections of the site suspected of being contaminated could not be accessed due to undergrowth. All measurements were taken under the supervision of SEPA.

Site access also provided a good opportunity to perform a supplementary HGS detector comparison alongside novel spectral processing techniques. The first detector, Sodium Iodide (NaI:Tl), was chosen as it is the workhorse of environmental gamma-ray spectrometry and in our previous work has proved effective at determining the depth and

activity of ^{226}Ra (Varley et al., 2015b). The second detector, Lanthanum Bromide (LaBr:Ce), has over the past decade received much interest since it provides better energy resolution (~2.5% at 662 keV) than the NaI:Tl (~7% at 662 keV) at the same time as offering similar robustness (Guss et al., 2010) (Fig. 4B). However, each LaBr:Ce spectrum presents a large number of background counts distributed throughout the spectrum owing to internal isotopes (^{138}La and ^{227}Ac) (Iltis et al., 2006). Although laboratory comparisons have been performed between these two detectors, limited field comparisons have been performed (Menge et al., 2007; Milbrath et al., 2007).

Over the course of four days, in excess of 25,000 spectra were collected using the two detectors (both 71 × 71 mm). To ensure that spectra acquired by each detector were comparable the detectors were attached to a wheel barrow system, offset longitudinally by 0.5 m and attached at a height of 0.1 m from the floor, to ensure the same ground was covered. 1024 channel spectra were acquired using Ortec's Maestro software every second together with GPS coordinates provided by an SX Blue II differential GPS with a 0.6 m positional accuracy. A walking speed of 0.5 m s^{-1} was maintained during the survey. Data were logged and displayed in real-time with Stirling Mobile Gamma Spectrometry System (SMoGSS), software developed in-house, which also provided alarms when spectra, suspected of containing contamination components, were acquired.

It was acknowledged to adequately characterise the contaminated areas of the site the background spectral population would have to also be accurately characterised to use as a baseline in later modelling. The site was chosen because it was made up of a similar geological composition and was immediately next to the site. Therefore, 10,000 spectra (approximately 30% of the entire dataset) were taken on the same day where weather conditions remained i.e. a clear day.

2.2. Monte Carlo Simulations

To obtain a representative detector spectral response for a given detector to homogeneous source geometry can be problematic if attempted through laboratory based calibrations (Maučec et al., 2004). This is due to complications associated with distributing a radioactive source and also obtaining one active enough to provide acceptable counting uncertainties at greater depths after subtraction of the background (Hendriks et al., 2002). Consequently, Monte Carlo Simulations (MCS) were used in this study since a homogeneous source could be accurately modelled (Allyson and Sanderson, 2001).

Source spectra containing 1024 channels (the same as field spectra) were generated using the software package Monte Carlo N-Particle 5 (MCNP5) (Briesmeister, 1993). It was acknowledged that a wide-range of source geometries may be present at the site; thus posing an intricate source population to model. Therefore, for simplicity the majority of contamination was assumed to be heterogeneously distributed and underneath an unknown uniform depth of relatively non-contaminated overburden. This permitted a simple two-layer cylinder model to be developed within MCNP5 (Fig. 3). The bottom layer (of thickness Z_c) was assumed to homogenously contaminate down to a depth of 0.8 m, and the thickness of the upper layer (Z_u) was altered to simulate increasing non-contaminated overburden (Thummerer and Jacob, 1998). Further information regarding the Monte Carlo routines used is provided in the supplementary materials (Appendix 1).

2.3. Dataset generation

In order to train and cross validate models, two synthetic spectral calibration datasets were produced: a training dataset and a cross-validation dataset. The training dataset comprised of spectra recorded to a low statistical counting uncertainty with well-defined spectral shape. This allowed for an optimised model to be fitted to systematic changes in detector response rather than counting noise. This

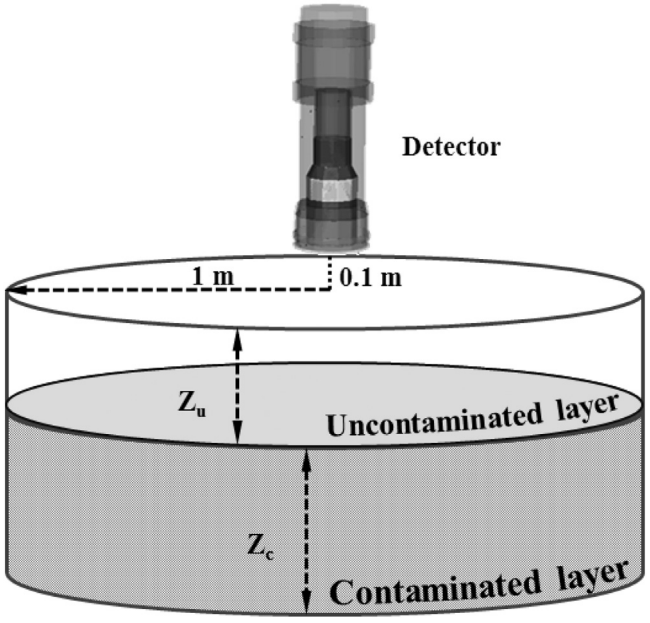

Fig. 3. Schematic diagram of the two-layer Monte Carlo model used to acquire source spectral responses.

encompassed taking relatively long background measurements (60 s) at different places on the background analogue site to produce a relatively well defined background spectrum. This collection of low uncertainty background spectra were then randomly spiked with Monte Carlo derived spectral response with a low statistical uncertainty (see Appendix 1 for details).

The cross-validation dataset was formed in much the same way as the training dataset, however, 1 s counts were obtained from the background analogue site and simulations with much higher counting uncertainties were used. The Monte Carlo regimes used to achieve this are described in the supplementary materials (Appendix 1). Resultantly, the cross-validation dataset contained a much larger noise component that was considered more representative of spectral responses collected in the field at the contaminated site. The purpose of this dataset was to ensure that models were not being over-fitted to the training dataset.

2.4. Spectral binning

HGS spectra obtained over 1 s tend to exhibit large counting uncertainty (Alamaniotis et al., 2013b) (Fig. 1B). In our previous work (Varley et al., 2015a) using NaI:Tl and LaBr:Ce we have found it more suitable to observe general changes in spectral shape by transforming each spectrum (1024 channels) into a smaller number of non-overlapping energy bins (typically 10–25 bins depending on the detector). This negates some counting noise without significant loss of energy differentiation (Jarman et al., 2008). Two binning methods were implemented. The first placed bins around Regions of Interest (ROIB) based on characteristic ^{226}Ra emissions and scattering regions (Fig. 4). The second more systematic approach, coined resolution binning (RB), developed bins based upon the deterioration of energy resolution with increasing energy (Runkle, 2006).

ROIB used on a NaI:Tl was shown to be the most effective detector setup in the routine monitoring of ^{226}Ra "hot" particles. However, this work is inherently different given that it is not practical to transform bins into the time series in order to negate local background changes as large areas were known to be homogeneously contaminated. Therefore, the employment of Principal Component Analysis to directly compare background and source could favour more bins (RB) and the superior energy resolution and energy efficiency of LaBr:Ce, since

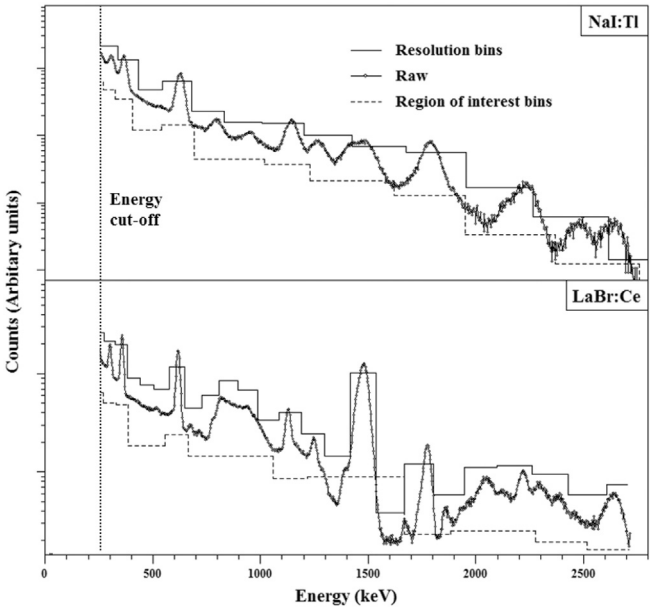

Fig. 4. Binning methods for NaI:Tl and LaBr:Ce detectors.

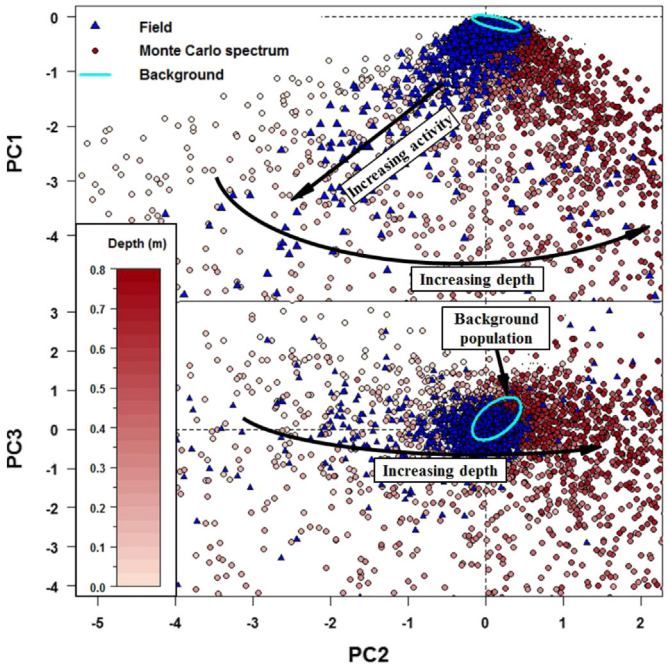

Fig. 5. Patterns within loadings from the PCs 1, 2 and 3 for NaI:Tl between Monte Carlo derived cross-validation set (circles) and field results (triangles). Notably, burial depth is separated within Principal Component space (yellow indicates surface and red buried) and increasing distance from the background population (Cyan ellipse — derived using mahalanobis distance) infer increases in activity. (For interpretation of the references to colour in this figure legend, the reader is referred to the web version of this article.)

counts from internal contamination may be suppressed more efficiently.

Importantly, energies below 250 keV were discarded from analysis given that large systematic variations take place on a spatial scale that can be very challenging to predict (Caciolli et al., 2012). This can be attributed to the photoelectric effect becoming the dominant form of photon interaction, which is controlled by the composition of the soil matrix (Tyler, 2008).

2.5. Principal Component Analysis

Principal Component Analysis (PCA) was employed to produce a set of noise reduced uncorrelated spectral shapes known as Principal Components (PCs) (Du et al., 2010). The mathematical routine used to derive this is presented in the supplementary materials (Appendix 2). Here a brief description is given.

Importantly, before the dataset was spectrally decomposed through PCA, each spectrum was noise adjusted to in an attempt to yield equal variance in all channels (Hovgaard, 1997). The process of PCA then orders subsequent PCs according to the total variance contributed to the dataset. Here, the assumption was taken that the majority of variance corresponds to source signal in the lower order PCs and uncorrelated counting noise in the higher order PCs (Hotelling, 1933). All but the first 3 PCs were then discarded, substantially reducing the dimensionality of the dataset and alleviating uncorrelated elements associated with counting noise (Runkle, 2006). Furthermore, spectral drift components were also separated out into higher order PCs. Patterns within the first 3 PC loadings, corresponding to signal, were then used to infer whether there were contributions from ^{226}Ra and at what depth and activity it was occurring (Adams et al., 2012) (Fig. 5).

PCA was performed on the entire dataset (training, cross-validation, and field spectra) to enable field spectra to be encompassed into the same PC structure as synthetic data (training and cross-validation datasets) providing a direct means of spectral comparison (Varley et al., 2015b) (Fig. 5). The intention behind this was for patterns contained within the synthetic spectral data to be modelled. This would then allow similar patterns within field spectral signals to be characterised using the same models, thus providing activity and depth estimates.

In general, notice that depth (angle from background population) and activity (distance from the background population) could be inferred from the first 3 PCs (Fig. 5). Importantly, the cyan ellipses (Fig. 5) indicate the location in PC space where 95% of the background population would occupy if background points were not concealed by overlying MC spectra. A detailed description of Mahalanobis distance (Appendix 3) can be found in the supplementary materials as it is used later as a classification algorithm.

This demonstrates a significant reduction in dimensionality (from 10 to 25 bins to a 3 PCs) whilst still maintaining a considerable proportion of the signal, therefore simplifying the later modelling process. However, non-linearities were presented within the PCA transformed data that can be problematic to model using convention regression and classification algorithms, such as non-linear regression (Adams et al., 2012) and Mahalanobis distance (Runkle, 2006).

2.6. Machine Learning

A solution to extracting significant patterns within PC loadings is offered by data-driven Machine Learning (ML) algorithms (Sharma et al., 2012). Providing there is sufficient data available to robustly train and cross-validate models, ML is able to fit to high dimensional, complex feature spaces (Fig. 5) where noise structure may differ from Gaussian. Recent developments in software have provided user-friendly development environments tailored towards practical application (Ao et al., 2010). For these reasons, ML has been used to interpret gamma-ray spectrometry data previously (Yoshida et al., 2002; Dragovic et al., 2005; Kangas et al., 2008; Wei et al., 2010; Sharma et al., 2012). Early exploration and previous experiences offered two promising ML methods: Neural Networks (NN) and Support Vector Machines (SVM) (Varley et al., 2015a). For detailed definitions and training procedures used on NNs (Apendix 4) and SVMs (Appendix 5) refer to the supplementary materials.

It was found early on to generate optimum performance for ML it was more suitable to divide the modelling task into two:

i) To classify PC loadings into source or background; and
ii) Apply a regression to provide depth and activity estimates.

Binary classification presents a trade-off between false positive and true positive rates, and as there was no predefined false positive rate, Receiver Operator Characteristics (ROC) was chosen as a robust measure of detection rate (T.J. Stocki et al., 2008). To quantify classification, the Area Under the Curve (AUC) of an ROC plot was calculated whereby values closer to one were considered better classifiers. To robustly test the classifiers, a uniform random sample of activities (0.1–2 Bq g^{-1}) and depth (0–0.8 m) was drawn to derive AUC from the cross validation set. Each ML algorithm was run 10 times on 10 independent randomly drawn datasets, which provided a standard deviation for the AUC. Notably, a field spectrum was only classified as being from the source class if the ML method identified that spectrum as being a source 5 or more times during the 10 individual runs.

Regression performance was assessed by calculating the r^2 value between model prediction and actual values on the cross validation set which was formed by a uniform random sample of activities (0.1–20 Bq g^{-1}) and depths (0–0.8 m) (Moreira et al., 2010). To ensure uncertainties on final estimates could be assessed for the final optimised model, it was fitted and cross-validated to 10 randomly drawn spiked dataset (Section 2.3) providing a standard error and mean for each field measurement. PCs were normalised to their mean and variance. Training and cross-validation datasets comprised of 2000 and 4000 data points, respectively.

3. Results and discussion

3.1. Spectral classification

The best classification results, independent of algorithm, detector, or binning method, were found by using the first 3 PCs. This is consistent with source signal being captured within these first few PCs and lower ordered PCs containing principally noise (Dickson, 2004). This result significantly reduced dimensionality and simplified detection. This could explain the reason why the number of hidden neurons was consistently below 10 and learning tended to converge around 4000 epochs for all optimal classification NNs. SVM gamma (300–1000) and cost (100–800) were relatively large implying the classification boundary required a close-fitting boundary that was highly dependent on individual training points (Meyer and Wien, 2014).

ML methods showed a significant improvement in AUC (0.793–0.840) over traditional Mahalanobis distance (0.786–0.792) (Table 1). This suggests the classification boundary was non-linear and so, a Gaussian assumption was too simplistic to accurately model the boundary, whereas the ML algorithms were capable to define these accurately. Of the two ML methods, NN (0.831–0.84) consistently outperformed SVM (0.793–0.824) for all detector configurations. However, patterns within the two binning systems are harder to explain since resolution binning produced better results for NaI:Tl whereas region of interest binning suited LaBr:Ce better. For LaBr:Ce this may be due to the alleviation in counting noise through fewer, logically placed, bins aiding in the de-noising process particularly in contaminated areas (Fig. 4b). NaI:Tl with almost no internal contamination, more bins may have providing more information in which to draw more representative PCs from.

In previous work where a real-time application was needed the internal contamination posed by LaBr:Ce was found to hinder its detection capabilities (Varley et al., 2015a). However, the ability to post-process data, and thus, negate the influence of intrinsic counts using a technique such as PCA demonstrated the superior energy resolution and efficiency of LaBr:Ce can still be utilised to provide improved detection rates over a s short count time. Another reason could be that in a real-time application a relatively large number of input dimensions are required (13 bins) to capture spectral shape changes. The smaller number of noise-reduced PCs (3 loadings) provided a clearer signal for ML to distinguish between.

Table 1
Area Under the Curve values for different detector, binning system and algorithm combinations. Abbreviations: Region of Interest Binning (ROIB), Resolution Binning (RB), Neural Networks (NN) and Support Vector Machines (SVM).

Algorithm	NaI:Tl		LaBr:Ce	
	Binning system		Binning system	
	RB	ROIB	RB	ROIB
Mahalanobis	0.788 ± 0.004	0.786 ± 0.006	0.785 ± 0.007	0.792 ± 0.005
NN	0.831 ± 0.005	0.830 ± 0.003	0.836 ± 0.004	0.840 ± 0.006
SVM	0.815 ± 0.003	0.793 ± 0.005	0.796 ± 0.006	0.824 ± 0.005

3.2. Depth and activity estimates

In keeping with the classification results, it was found that using the first 3 PCs as inputs produced the lowest r^2 values for all NNs. Ten-to-15 thousand learning epochs were found to be adequate to train all NNs. More neurons were needed for resolution binning (18–20), in comparison to region of interest binning (10–15), suggesting the structure of data in the feature space was slightly more complex for resolution binning.

Consistently higher r^2 values, for activity and depth, using either binning system, were found for LaBr:Ce (0.738–0.752 and 0.590–0.608, respectively) when compared to NaI:Tl (0.691–0.696 and 0.527–0.544, respectively). Noteworthy, all p-values for r^2 values were significant (<0.005). This further supported the argument that the superior energy resolution and efficiency of LaBr:Ce could be utilised for environment monitoring on condition that there is enough training data to implement a post processing algorithm (such as PCA) to lessen the effect of nuisance signals from internal contamination. For HGS monitoring where real-time output is required, NaI:Tl is probably still the most reliable detector. Again using fewer, more systematically placed energy bins (ROIB), provided higher performance.

Fig. 6 provides some insight into the inner workings of the overall approach. For instance, the lower activity (0.1 Bg g^{-1}) surface (2 cm) source presents clear peaks in the lower energy region of the spectrum (notice the dominant 609 keV peak in both the raw and binned spectra) as photons have not been significantly attenuated by the small distance of soil they have had to travel through. Conversely, the spectrum

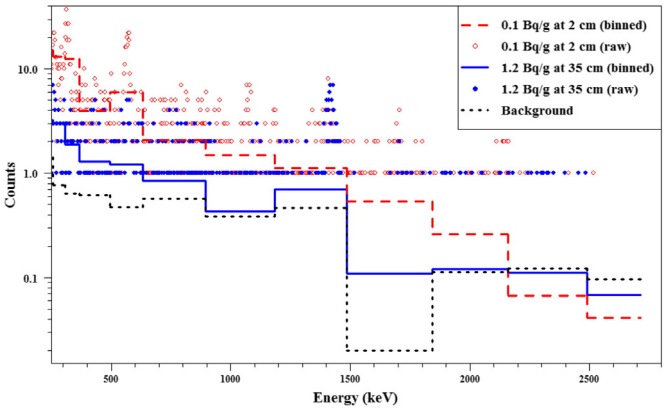

Fig. 6. Neural network estimations of 3 different spectra obtained using the lanthanum bromide detector: low activity (0.1 Bg g^{-1}) at the surface (2 cm depth), high activity (1.2 Bg g^{-1}) at depth (35 cm) and background. The raw data (1024 channels) has also been provided alongside binned source spectra for comparison.

estimated to be at greater depth (35 cm) at greater activity (1.2 Bq g^{-1}) the spectrum appears more flat as many of the lower full energy photons have been attenuated by the thicker mass of soil; resulting in a reduction in lower energy peaks. However, comparing the higher energy bin containing the 1764 keV peak, and significant amount of low energy scatter, to the background spectrum, provides evidence for a much deeper contamination.

3.3. Analysis of case study site

Spectral classification and regression of field data was performed using two NN on region of interest binning-LaBr:Ce spectra. Activity and depth estimates of source spectra demonstrate the advantages the approach (Fig. 7). The majority of highest activity contamination (>1 Bq g^{-1}) was estimated to be buried beyond 0.2 m, with the highest activities occurring at greater depths (0.3–0.5 m). Hotspots identified during the survey using straightforward gross counting (red colours), although they represent the highest surface dose rates they were relatively low activity (<1 Bq g^{-1}) positioned at the surface (<0.05 m).

Another feature is the exponentially increasing manner of the activity of detected source spectra with greater depth (Fig. 7). This represents the limit of detection, beyond these depths ^{226}Ra could not be confidently separated from background by the classification NN. Notice that the standard error for measurements generally increases with greater depth. This can be attributed to fewer source counts across the spectrum producing a lower signal to noise ratio making the fitting procedure more difficult for the regression NN.

In this scenario, results would have to be treated with considerable caution. To potentially validate its presence, neighbouring measurements should be analysed to see if there was an extended layer present or the measurement was isolated contamination. In the event of a significant isolated measurement, further measurements would have to be taken, in that area, at a later time, to validate its presence. This could take place alongside intrusive investigations. Nonetheless, these types of scenario present a considerable challenge to circumvent using remote gamma-ray measurements.

Contamination at this site could not be identified beyond 0.6 m using the method, because at these depths, much higher activities would have been beyond the limit of detection (Fig. 7). This reflects the ultimate limitation of in situ and mobile gamma-ray spectrometry. Crucially though, this type of method could be used as the first tool to rapidly survey a site, where hotspots, potentially at depth, could be identified for later intrusive work. Naturally, to gain a better assessment of deeper contamination identified by the technique, borehole measurements could be taken and a similar spectral processing approach could be applied (Varley et al., 2015b). Alternatively, longer counting times using a higher resolution detector, for instance a High Purity Germanium detector, could be implemented; potentially improving overall detection accuracy. Importantly, all of these approaches could be applied prior to labour intensive soil sampling.

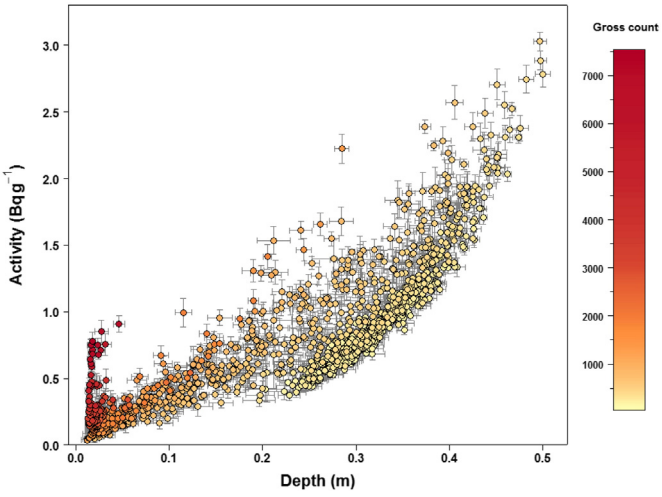

Fig. 7. Activity and depth estimates alongside standard error for source spectra from field site. Colour ramp indicates gross count rate. (For interpretation of the references to colour in this figure legend, the reader is referred to the web version of this article.)

In addition, the case study provided evidence that the critical value for the exemption of Naturally Occurring Radioactive Material (above 10 Bq g^{-1}) is not exceed at the site at less than 0.6 m.

An interesting section of the site (graphical abstract), consisting of an area of ground approximately 600 m^2 in size, has been characterised and spatially smoothed using inverse distance weighting (Shepard, 1968). This area displays a large variation in activity, depth and lateral distribution of contamination. Notice how the highest intensity gross counting hotspots (red sections on upper plot) correspond to relatively low activity (>0.01 Bq g^{-1} or green areas) that are close to the surface (>0.05 cm). However, there tends to be much higher contamination at greater depths (Fig. 7) in the close vicinity of these areas (pink areas in the foreground). An explanation for this is that hotspots may represent the latest (less contaminated) spoil, laid down at the end of the formation of the tip (ash and clinker can been seen at surface on some of the hotspots). Much higher concentrations of ^{226}Ra would appear to have been laid down earlier in the history of the site, perhaps during and immediately after the Second World War when large ^{226}Ra inventories were being disposed of. This contamination occurs at greater depths under a relatively non-contaminated overburden, which is likely to have been used to cover contamination at a later date.

4. Conclusions

A method employing Principal Component Analysis and Neural Networks was developed and applied for rapid estimation of the depth and activity of homogeneous ^{226}Ra contamination from surface measurements taken using handheld gamma-ray detectors. This enables the accurate characterisation of an area contaminated with ^{226}Ra and interpolated maps of the processed data ultimately allow for the risk to human health, in both long and short term, to be robustly assessed. The superior energy resolution of LaBr:Ce resulted in better depth and activity resolving capability demonstrated that it was more suitable than the standard NaI:Tl for this type of contaminated land application and could easily be applied to other gamma emitting radionuclides such as ^{137}Cs.

Acknowledgements

This work was funded by NERC (project — NE/I018956/1) and Nuvia Limited (project — 46007/008). We would like to thank Mark Toner and Christopher Sneddon for assisting in field data acquisition and Nuvia Limited for providing the Lanthanum Bromide detector. We would also like to thank a number of anomalous reviewers for their useful suggestions that significantly improved the accessibility of the manuscript.

Appendix A. Supplementary data

Supplementary data to this article can be found online at http://dx.doi.org/10.1016/j.scitotenv.2015.10.112.

References

Adams, J.C., Joyce, M.J., Mellor, M., 2012. The advancement of a technique using principal component analysis for the non-intrusive depth profiling of radioactive contamination. IEEE Trans. Nucl. Sci. 59, 1448–1452.

Adsley, I., Davies, M., Murley, R., Pearman, I., Scirea, M., 2004. 3D GPS mapping of land contaminated with gamma-ray emitting radionuclides. Appl. Radiat. Isot. 60, 579–582.

Alamaniotis, M., Hernandez, H., Jevremovic, T., 2013a. Application of support vector regression in removing Poisson fluctuation from pulse height gamma-ray spectra. pp. 1–4.

Alamaniotis, M., Heifetz, A., Raptis, A.C., Tsoukalas, L.H., 2013b. Fuzzy-logic radioisotope identifier for gamma spectroscopy in source search. IEEE Trans. Nucl. Sci. 60, 3014–3024.

Allyson, J.D., Sanderson, D.C.W., 2001. Spectral deconvolution and operational use of stripping ratios in airborne radiometrics. J. Environ. Radioact. 53, 351–363.

Ao, S., Rieger, B.B., Amouzegar, M.A., 2010. Machine learning and systems engineering. Springer.

Beck, H., De Campo, J., Gogolak, C., 1972. In situ Ge (Li) and Na (Tl) gamma-ray spectrometry. US Department of Energy, Environmental Measurements Laboratory, HASL-258, New York.

Briesmeister, J.F., 1993. MCNP-A general Monte Carlo N-particle transport code. LA-12625.

Caciolli, A., Baldoncini, M., Bezzon, G.P., Broggini, C., Buso, G.P., Callegari, I., et al., 2012. A new FSA approach for in situ γ ray spectroscopy. Sci. Total Environ. 414, 639–645.

Dale, P., Gemmill, J., Milne, J., 2013. Dalgety bay radioactive contaminated land risk assessment. Radioactive Substances, Scottish Environmental Protection Agency, pp. 1–91.

DECC, 2012. Radioactive Contaminated Land Statutory Guidance Environmental Protection Act 1990: Part 11A. Contaminated Land. Area 3C, 3 Whitehall Place, London, pp. 1–70.

Dickson, B.L., 2004. Recent advances in aerial gamma-ray surveying. J. Environ. Radioact. 76, 225–236.

Dragovic, S., Onjia, A., Stankovic, S., Anicin, I., Bacic, G., 2005. Artificial neural network modelling of uncertainty in gamma-ray spectrometry. Nucl. Instrum. Methods Phys. Res., Sect. A 540, 455–463.

Du, Q., Wei, W., May, D., Younan, N.H., 2010. Noise-adjusted principal component analysis for buried radioactive target detection and classification. IEEE Trans. Nucl. Sci. 57, 3760–3767.

Fagan, D.K., Robinson, S.M., Runkle, R.C., 2012. Statistical methods applied to gamma-ray spectroscopy algorithms in nuclear security missions. Appl. Radiat. Isot. 70, 2428–2439.

Guastaldi, E., Baldoncini, M., Bezzon, G., Broggini, C., Buso, G., Caciolli, A., et al., 2013. A multivariate spatial interpolation of airborne γ-ray data using the geological constraints. Remote Sens. Environ. 137, 1–11.

Guss, P., Reed, M., Yuan, D., Cutler, M., Contreras, C., Beller, D., 2010. Comparison of $CeBr_3$ with $LaBr_3$:Ce, $LaCl_3$:Ce, and NaI:Tl detectors. Hard X-Ray, Gamma-Ray, and Neutron Detector Physics Xii 7805.

Haddad, K., Al-Masri, M.S., Doubal, A.W., 2014. Determination of 226Ra contamination depth in soil using the multiple photopeaks method. J. Environ. Radioact. 128, 33–37.

Hendriks, P., Limburg, J., De Meijer, R., 2001. Full-spectrum analysis of natural γ-ray spectra. J. Environ. Radioact. 53, 365–380.

Hendriks, P.H.G.M., Maučec, M., de Meijer, R.J., 2002. MCNP modelling of scintillation-detector γ-ray spectra from natural radionuclides. Appl. Radiat. Isot. 57, 449–457.

HMSO, 1996. CM 2919 (1995) Review of Radioactive Waste Management Policy-Final Conclusions.

Hotelling, H., 1933. Analysis of a complex of statistical variables into principal components. J. Educ. Psychol. 24, 417.

Hovgaard, J., 1997. Airborne gamma-ray spectroscopy. Airborne Gamma-ray Spectrometry (PhD Thesis).

IAEA, 1998. Characterization of radioactively contaminated sites for remediation purposes.

IAEA, 2003. Guidelines for radioelement mapping using gamma ray spectrometry data. Nuclear Fuel Cycle and Materials Section. International Atomic Energy Agency, Vienna, pp. 1–173.

Iltis, A., Mayhugh, M.R., Menge, P., Rozsa, C.M., Selles, O., Solovyev, V., 2006. Lanthanum halide scintillators: properties and applications. Nucl. Instrum. Methods Phys. Res., Sect. A 563, 359–363.

Jarman, K.D., Runkle, R.C., Anderson, K.K., Pfund, D.M., 2008. A comparison of simple algorithms for gamma-ray spectrometers in radioactive source search applications. Appl. Radiat. Isot. 66, 362–371.

Kangas, L.J., Keller, P.E., Siciliano, E.R., Kouzes, R.T., Ely, J.H., 2008. The use of artificial neural networks in PVT-based radiation portal monitors. Nucl. Instrum. Methods Phys. Res., Sect. A 587, 398–412.

Knoll, G.F., 2010. Radiation detection and measurement. John Wiley & Sons.

Kock, P., Lanke, J., Samuelsson, C., 2012. A real-time statistical alarm method for mobile gamma spectrometry—combining counts of pulses with spectral distribution of pulses. Nucl. Instrum. Methods Phys. Res., Sect. A 681, 55–60.

Maučec, M., de Meijer, R.J., van der Klis, M.M.I.P., Hendriks, P.H.G.M., Jones, D.G., 2004. Detection of radioactive particles offshore by γ-ray spectrometry part II: Monte Carlo assessment of acquisition times. Nucl. Instrum. Methods Phys. Res., Sect. A 525, 610–622.

Menge, P.R., Gautier, G., Iltis, A., Rozsa, C., Solovyev, V., 2007. Performance of large lanthanum bromide scintillators. Nucl. Instrum. Methods Phys. Res., Sect. A 579, 6–10.

Meyer, D., Wien, F.T., 2014. Support vector machines. The Interface to libsvm in package.

Milbrath, B.D., Choate, B.J., Fast, J.E., Hensley, W.K., Kouzes, R.T., Schweppe, J.E., 2007. Comparison of LaBr3:Ce and NAI(Tl) scintillators for radio-isotope identification devices. Nucl. Instrum. Methods Phys. Res., Sect. A 572, 774–784.

Miller, K.M., Shebell, P., Klemic, G.A., 1994. In-situ gamma-ray spectrometry for the measurement of uranium in surface soils. Health Phys. 67, 140–150.

Moreira, M.C.F., Conti, C.C., Schirru, R., 2010. A new NaI(Tl) four-detector layout for field contamination assessment using artificial neural networks and the Monte Carlo method for system calibration. Nucl. Instrum. Methods Phys. Res., Sect. A 621, 302–309.

Pratt, R., 1993. Review of radium hazards and regulation of radium in industry. Environ. Int. 19, 475–489.

Read, D., Read, G., Thorne, M., 2013. Background in the context of land contaminated with naturally occurring radioactive material. J. Radiol. Prot. 33, 367.

Runkle, R., 2006. Analysis of spectroscopic radiation portal monitor data using principal components analysis. IEEE Trans. Nucl. Sci. 53, 1418–1423.

Sharma, S., Bellinger, C., Japkowicz, N., Berg, R., Ungar, K., 2012. Anomaly detection in gamma ray spectra: a machine learning perspective. IEEE Symposium on Computational Intelligence for Security and Defence Applications (CISDA), 2012. IEEE, pp. 1–8.

Shepard, D., 1968. A two-dimensional interpolation function for irregularly-spaced data. Proceeding ACM '68 of the 1968 23rd ACM national conference, pp. 517–524.

Statutory Guidance to support the Radioactive Contaminated Land (Scotland) Regulations, 2008d. http://www.scotland.gov.uk/Publications/2008/03/31102033/0; (2015).

Stebbings, J.H., 2001. Health risks from radium in workplaces: an unfinished story. Occup. Med. (Philadelphia, Pa.) 16, 259–270.

Stocki, T.J., Japkowicz, N., Li, G., Ungar, R.K., Hoffman, I., Yi, J., 2008. Summary of the Data Mining Contest for the IEEE International Conference on Data Mining, Pisa, Italy 2008. p. 1.

The Radioactive Substances Act 1993 Amendment (Scotland) Regulations, 2011a. http://www.legislation.gov.uk/sdsi/2011/9780111012758/introduction (January, 2015).

Thummerer, S., Jacob, P., 1998. Determination of depth distributions of natural radionuclides with in situ gamma-ray spectrometry. Nucl. Instrum. Methods Phys. Res., Sect. A 416, 161–178.

Tyler, A.N., 2008. In situ and airborne gamma-ray spectrometry. Anonymous Radioactivity in the Environment. Elsevier, pp. 407–448.

Tyler, A., Dale, P., Copplestone, D., Bradley, S., Ewen, H., McGuire, C., et al., 2013. The radium legacy: contaminated land and the committed effective dose from the ingestion of radium contaminated materials. Environ. Int. 59, 449–455.

Varley, A., Tyler, A., Smith, L., Dale, P., Davies, M., 2015a. Remediating radium contaminated legacy sites: advances made through machine learning in routine monitoring of "hot" particles. Sci. Total Environ. 521, 270–279.

Varley, A., Tyler, A., Smith, L., Dale, P., 2015b. Development of a neural network approach to characterise ^{226}Ra contamination at legacy sites using gamma-ray spectra taken from boreholes. J. Environ. Radioact. 140, 130–140.

Wei, W., Du, Q., Younan, N.H., 2010. Particle swarm optimization based spectral transformation for radioactive material detection and classification. IEEE International Conference on Computational Intelligence for Measurement Systems and Applications (CIMSA), 2010, pp. 1–6.

Wilson, C.A., Adderley, W.P., Tyler, A.N., Dale, P., 2013. Characterising the morphological properties and surface composition of radium contaminated particles: a means of interpreting origin and deposition. Environ. Sci. Process. Impacts 15, 1921–1929.

Yoshida, E., Shizuma, K., Endo, S., Oka, T., 2002. Application of neural networks for the analysis of gamma-ray spectra measured with a Ge spectrometer. Nucl. Instrum. Methods Phys. Res., Sect. A 484, 557–563.